Experimental and numerical characterization of a mechanical expansion process for thin-walled tubes

Experimental and numerical characterization of a mechanical expansion process for thin-walled tubes

Massimiliano Avalle [a], Paolo Claudio Priarone [b], Alessandro Scattina [a, *]

[a] Politecnico di Torino, Department of Mechanical and Aerospace Engineering,

Corso Duca degli Abruzzi 24, 10129 Torino, Italy

[b] Politecnico di Torino, Department of Management and Production Engineering,

Corso Duca degli Abruzzi 24, 10129 Torino, Italy

*** Corresponding Author (A. Scattina)**

Phone: +39 011 0906913

Fax: +39 011 0906999

Email: alessandro.scattina@polito.it

Abstract

Air heat exchangers are made with tubes joined to finned pack. The connection between tubes and fins can be obtained through a mechanical process where an ogive is pushed inside the tube with smaller internal diameter causing its expansion. Residual plastic deformation provides the assembly with the fins. Accurate connection over the whole contact area of the tubes and fins is essential for maximum heat exchange efficiency. The goal of this work is to study and develop a finite element model able to effectively simulate expansion forming, allowing process analysis and, eventually, process optimization. The paper is divided into a first experimental part, where the materials used for the heat exchangers are characterized, and a second numerical part where models have been developed on the basis of the experimental data. The developed models are used to identify the material properties with an inverse method, and then to study the technological process of tube expansion by using a simplified but sufficiently accurate description. The model has proved to be an effective design tool, as it can evaluate the influence of the main parameters on the process and so optimize production according to technological variations.

Keywords: mechanical tube expansion forming, process analysis, experimental characterization, FEM simulation

1. Introduction

In air heat exchangers production, tubes often made of copper and nickel alloys are joined to finned packs. The connection between tubes and fins must provide complete contact in order to ensure maximum heat exchange between the fluids that pass through the parts. The assembly is usually obtained through tube deformation, by means of hydraulic or mechanical expansion processes. In the first case, the manufacturing route uses a fluid medium conveyed inside the tube using high internal pressure. In the second case, an axisymmetric tool whose outer diameter is greater than the internal diameter of the tube, is pushed inside the tube. Eventually the permanent deformation caused by the tube expansion creates the assembly by interference of the tube with the front plates and the fins. For the mechanical process, there are two ways: one use a ball pushed by high pressure water and another use truncated-cone-nose ogive derived by mechanical actuator.

Previous analytical models have been developed by many authors, as summarized by Nadai (1950). In recent years, the analytical model developed by Karrech and Seibi (2010) allows the prediction of the driving force, the dissipated energy and the ogive angle, and it has been validated by finite element analysis. Almeida et al. (2006) refreshed and extended the fundamentals of tube expansion and reduction using a die, by means of comprehensive theoretical and experimental investigation. They defined the formability limits of this process: ductile fracture, local buckling and wrinkling. Tang et al. (2008) proposed a complete study of the expansion process where a thick walled microgroove copper tube is joined to aluminium fins. The results indicate that thermal-mechanical performance is mainly influenced by the expanding ratio. Tang et al. (2009) conducted FEM analysis, supported by experimental investigations, to study the effect of groove shape on forming quality. The outcome shows that the groove height reduction is heavily affected by the helix angle. The same approach was used by Alves et al. (2006) to study the influence of process parameters on the formability limits due to ductile fracture and wrinkling. The influence of expansion parameters on stress levels has been studied by Seibi et al. (2011) for aluminium and steel tubes examining expansion forces and the spring back phenomenon. Tang et al. (2011) have developed an FE model to improve the tube-fin contact of heat exchangers. The FE method has also been used to investigate a real tube sheet fracture, as proposed by Li et al. (2010).

In this context, the aim of this work is to describe a comprehensive step-by-step procedure to analyse the forming process of the expansion, which starts from the material characterization and concludes with a finely tuned simulation of the complete expansion process. The model allows the in depth evaluation of the influence of the main process parameters. As a result, a detailed analysis of the expansion phenomenon is shown, which highlights the dependence of most important material and process related parameters.

This paper is divided into a first experimental part, dedicated to the material analysis and to the expansion process study, and a second numerical part, with the development of FE models on the basis of the obtained data.

.

2. Experiments for material properties and driving force

2.1 Material properties

Different tensile tests were performed in order to study the mechanical properties of the tubes. The tests were carried out in accordance with the ASTM E8M-98 (1998) standard for tube specimen by means of an Instron 8801 testing machine. The tubes were in Cu-Ni alloy, the overall tube length L was 208-210 mm, and the external diameter was fixed to D_e = 15.85 mm (non-expanded tube). On the whole, four different types of samples were examined:

- 2 tube thickness values: t_0 = 1.0 and t_0 = 1.5 mm;
- 2 process grades: non-expanded and expanded.

The tests were performed in stroke control, and conducted to bring the samples up to failure in tension. In order to investigate the strain-rate effect, three loading speeds were examined: v = 0.1, v = 5 and v = 100 mm/s. In accordance to the test standard ASTM E8M-98 (1998), a steel plug was inserted into both ends of the samples to avoid collapse of the section when the tube is laterally compressed by the grips of the testing machine.

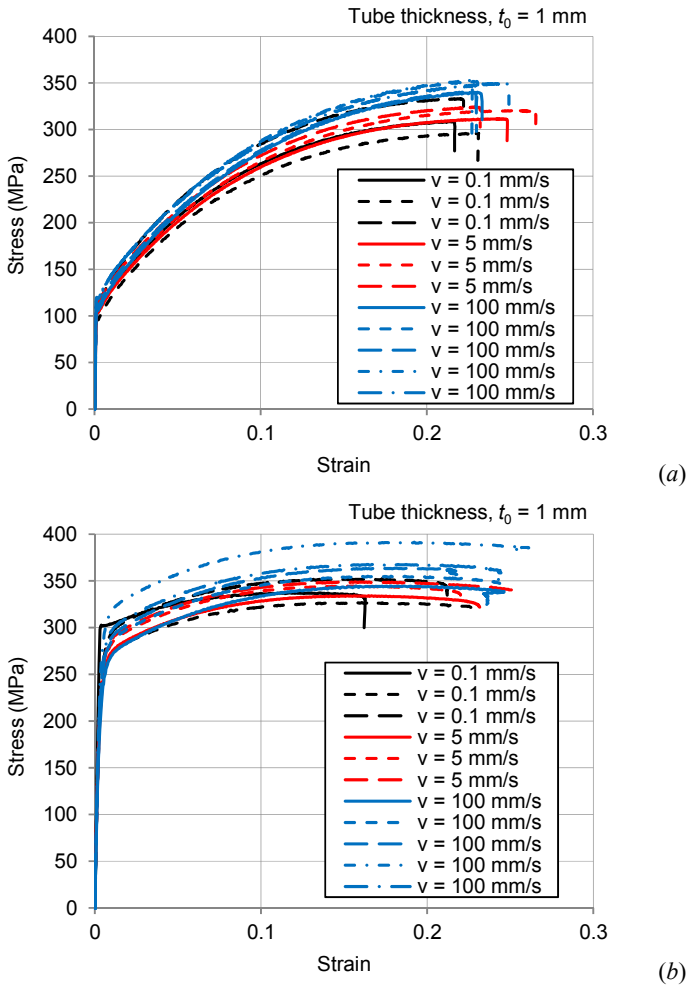

Fig. 1. Stress-strain characteristics for the non-expanded (*a*) and expanded (*b*) samples, with thickness t_0 = 1 mm.

The results in terms of stress-strain curves are presented in Fig. 1: the graphs refer to the case t_0 = 1 mm. For both the non-expanded and expanded tube conditions, results from loading at the three different speeds are shown. The obtained curves show that the yield stress in the expanded tubes is more than twice the yield stress in the non-expanded tubes. Conversely, non-expanded tubes show a greater amount of strain hardening. The results confirm that the material has moderate strain-rate sensitivity: nevertheless, if variations are not so significant, in the range of strain-rates typical of the studied process, the strain-rate sensitivity was included in the model of the material. In particular the Cowper-Symonds model (constants c and p in Table 1) was used as discussed in section 3.1.

2.2 Driving force

To acquire reference data for the development of the numerical models, and for the sensitivity analysis, experiments reproducing the production route were performed. Due to the complexity of the equipment used to manufacture the heat exchanger, which did not allow for a direct measurement of the process parameters, a simplified test equipment was designed and used. Two different experimental set of tests were defined: (1) the mechanical expansion of unconstrained (free) tubes, and (2) the mechanical expansion of tubes constrained by a simplified dummy exchanger. As for the previous tests, the wall thickness was t_0 = 1 mm and t_0 = 1.5 mm, and the insertion speed was v = 10 mm/s (for the unconstrained tubes only) and v = 100 mm/s. Grease, applied over the ogive surface, was used to insure proper lubrication. Finally, at least three repetitions of each test were performed.

In the first set of tests, the unconstrained tube was clamped at one end by one of the grips of the testing machine, whereas the ogive was inserted into the other end of the tube, as shown in Fig. 2. However, a pre-forming of the tubes is used in the process. Pre-forming slightly enlarges the first 10 mm in length, leaving a series of wrinkles. These wrinkles, as it will be shown later in section 3.2, affect the results in terms of the measured insertion force.

In the second set of tests, tubes to be expanded were constrained in the dummy heat exchanger, which is a small assembly reproducing the construction of a typical heat exchanger with six tubes arranged in a hexagonal pattern around the central tube (the tube to be expanded). Normal production plate fins were used to build this assembly, shown in Fig. 3. Again, the central tube was clamped by one grip of the testing machine, and the ogive was inserted in the other end of the tube. This second set of tests was aimed to be more representative of the real production process. These tests were performed at the greater speed of v = 100 mm/s only, this speed being close to the expansion speed used in the real production process. The experimental results are presented in Section 3.2, compared with the numerical results.

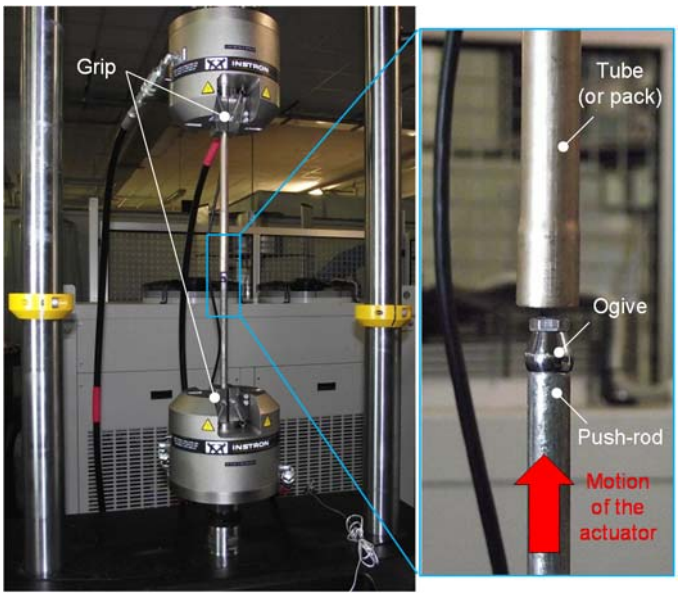

(*a*)

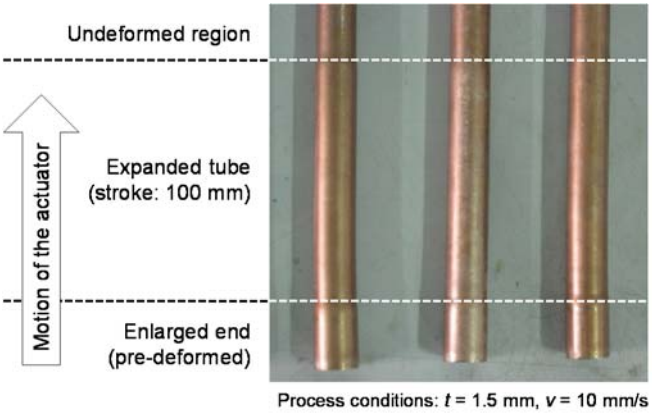

(*b*)

Fig. 2. Test method for the mechanical expansion measurement on the unconstrained tube (*a*). The picture (*b*) shows specimens at the end of the test.

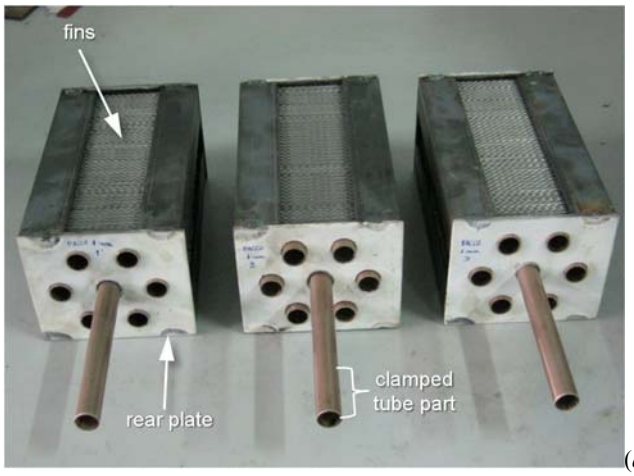

(*a*)

(*b*)

Fig. 3. Tube packs, wall thickness t_0 = 1mm.
The view (*a*) shows the end clamped in the machine grips; the other end (*b*) is the expanded end.

3. Simulation of the forming process

3.1 Modelling

The LS-DYNA 971 solver software, double precision version 6, was adopted for the finite element analysis. The implicit version of the solver was used.

Simulations of the tensile tests (described in Section 2.1) on both the expanded and non-expanded tubes were performed. The simulations of the tensile tests of the non-expanded tubes were aimed to identify the parameters of the material model. The simulations of the tensile tests of the expanded tubes served mainly as a validation of the material models. The latter were performed in a two-step process: first, the simulation of the tube expansion, and subsequently the tensile test itself. The first step is necessary to obtain the state of residual stress and strain that remains in the expanded tube, which affects the material behaviour during the tensile test on the expanded tube.

Different material models among the wide range of possibilities in the library of LS-DYNA (LS-DYNA Keyword User's Manual, 2007) were taken into consideration. At the end of this analysis, an elastic viscoplastic material model with thermal effects was chosen. The uniaxial stress-strain characteristic of the model is given by Eq. 1, where σ_0 is the yield stress, ε_{eff} is the effective plastic strain, $Q_{r1,2}$ and $C_{r1,2}$ are isotropic hardening parameters, $Q_{\chi 1,2}$ and $C_{\chi 1,2}$ are kinematic hardening parameters. In this model the viscous effects are accounted for using the Cowper and Symonds model (Cowper and Symonds 1957).

$$\sigma\left(\varepsilon_{eff}^{p}\right)=\sigma_{0}+Q_{r1}\left(1-\exp\left(-C_{r1}\varepsilon_{eff}^{p}\right)\right)+Q_{r2}\left(1-\exp\left(-C_{r2}\varepsilon_{eff}^{p}\right)\right)+Q_{\chi 1}\left(1-\exp\left(-C_{\chi 1}\varepsilon_{eff}^{p}\right)\right)+ \\ +Q_{\chi 2}\left(1-\exp\left(-C_{\chi 2}\varepsilon_{eff}^{p}\right)\right) \qquad \text{(Eq. 1)}$$

The parameters of the material model, listed in Table 1, were obtained by the inverse method process, by comparing the numerical with the experimental results and minimizing the difference between the two obtained curves.

Material model parameter	**Value**
Yield stress σ_0 (MPa)	102
Isotropic hardening parameters Q_{r1} (MPa)	360
Isotropic hardening parameters C_{r1}	9
Cowper and Symonds constant c (s^{-1})	33.8
Cowper and Symonds constant p	1.6

Table 1. FE material model parameters.

The tensile tests were simulated for both thicknesses, and for the three different velocities (v = 0.1, 5, and 100 mm/s), in order to consider the strain-rate effect.

Successively, the two sets of tests of the expansion process were studied. An axisymmetric solid model was adopted for these simulations by exploiting the geometrical properties of the specimen which is symmetric around the longitudinal axis. Hence, the cross section along the longitudinal axis was modelled with axisymmetric plane elements. This type of model allowed a consistent reduction of calculation time compared to a model with solid elements. However, the real tubes are far from being geometrically perfect, showing a certain amount of deviation from the ideal shape due to the lack of coaxiality between the ideal internal and external cylinder. A detailed analysis of the tube sections also revealed that the two surfaces are not perfect cylinders but are generated from elliptical profiles. This can induce manufacturing defects, and it can also cause additional problems in modelling. Nevertheless, such deviations from the ideal geometry were still sufficiently small to be neglected, and therefore a simple axisymmetric model can be used.

The average element size for this simulation was 0.125 mm, with 8 or 12 elements through the wall thickness of $t_0 = 1$ mm and $t_0 = 1.5$ mm, respectively. The model consisted of around 13000 for $t_0 = 1$ mm and 20000 for $t_0 = 1.5$ mm elements. The mesh of the ogive was built employing the same principle, using axisymmetric elements, and a rigid material model was adopted. The friction between the tube and ogive was fixed to $f = 0.15$. This value was chosen as a result of previous experiments carried out by the authors.

The boundary conditions were applied as close to the experimental tests as possible. For the simulation of the expansion of the unconstrained tubes, the model of the ogive and the first part of the tube are shown in Fig. 4 *a*: the first line of nodes (on the right) was constrained in the axial direction *Y*, which closely follows what happens in the process.

In the simulations of the assembled tubes, this model was completed by adding the fins, using the same axisymmetric hypothesis, as shown in Fig. 4 *b*. The average element size used for the fins was 0.075 mm. For the plate fins, an elasto-plastic material model was adopted. The parameters for the material model were obtained from experimental data of tests made on the aluminium alloy. The ends of the tube opposite to the ogive insertion were constrained for a length of 45 mm in all the degrees of freedom, as in the experimental tests. The ogive was subjected to constant velocity, equal to the velocity imposed in the tests of $v = 100$ mm/s. The fins were fully constrained on the external side, opposite to the tube wall. The fins were not joined together but contact was imposed between them, as in the real case.

3.2 Validation

The comparison between the experimental and the numerical results of the expansion process, in terms of the driving force as a function of the stroke is shown in Fig. 5 for both the considered thicknesses ($t_0 = 1$ mm and $t_0 = 1.5$ mm).

The experimental tests (Fig. 5*a*) highlight a slight influence of the loading speed, that can be attributed to the strain-rate sensitivity of the material. The results reveal two distinct behaviours. Initially, the ogive moves in the first part of the tube which is affected by the wrinkles: this causes the ripples in the load curve. In fact, the wavelength of these ripples

is the same for all the samples because they depend on the same wrinkle pattern. The deformation due to the wrinkles, although small in extent, induces some hardening in the material. Afterwards, the ogive travels in the undeformed tube, of nominally uniform constant section, and, consequently, it results in a constant driving force. Test repeatability is quite high, for both thicknesses and at both motion speeds of the ogive. In Fig. 5 *b*, differently from the simple single tubes, there is much more variability. The observation of resulting graphs clearly confirms this statement: the scatter increases distinctly after the first phase (corresponding to the initial tube wrinkling). The observed uncertainty is much more important in the thinner (t_0 = 1 mm) tubes. This is not easily explained: probably, the thinner tubes are more influenced by the plate fins, due to their lower rigidity. Moreover, the load slightly increases with stroke: this can be attributed to the limited length of the tested tubes. The further the ogive progresses through the tube, the less undeformed tube remains. The undeformed tube is compressed and locked at the opposite end: this somewhat influences the deformation process during its development.

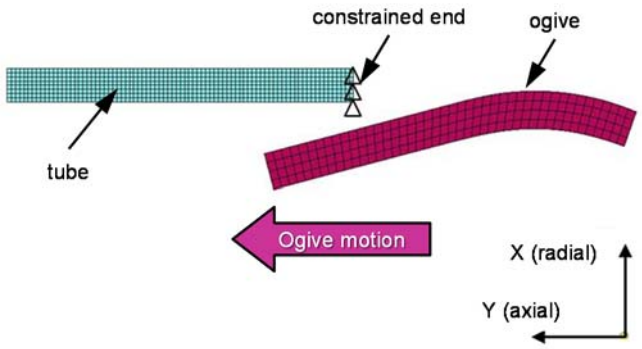

(*a*)

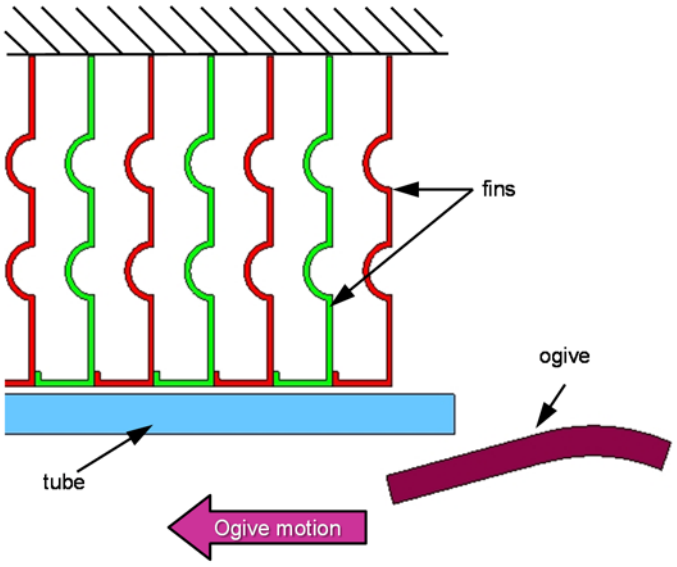

(*b*)

Fig. 4. Numerical model for the simulation of tube expansion for the unconstrained tube (*a*) and for the tube pack (*b*).

The results obtained with the FE models presented a good agreement with the experimental results in terms of the driving force. The numerical load curve showed some irregularities due to numerical approximations. The simulation results, in Fig. 5 *b* show the same slight force increase with increasing stroke. This is probably due to the packaging of the fins during the expansion process and to the limited length of the tested tubes.

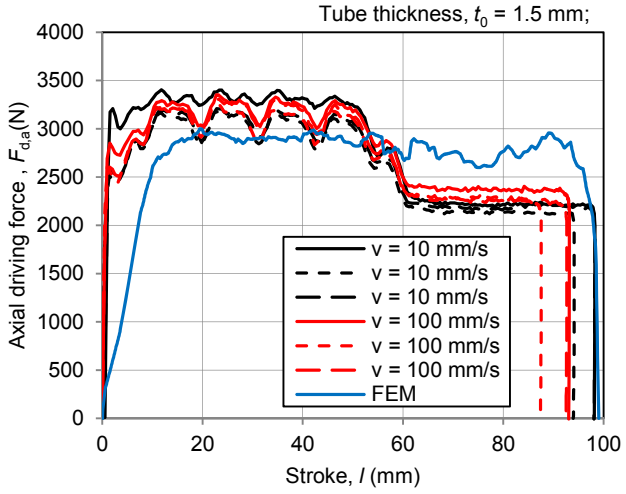

(*a*)

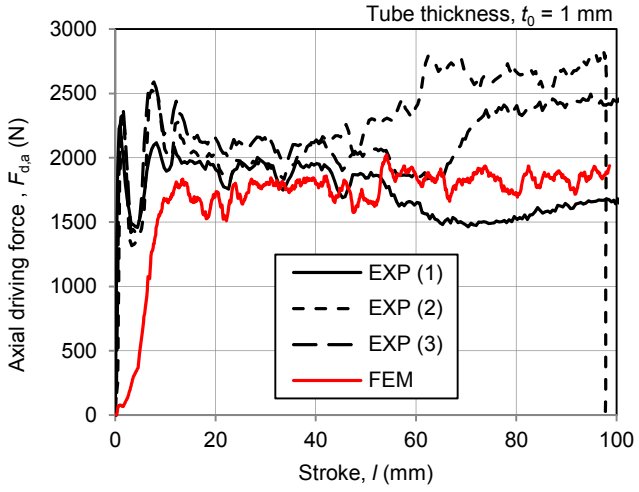

(*b*)

Fig. 5. Comparison between numerical and experimental measures of the axial driving force for the unconstrained tube (*a*) and for the tube pack (*b*).

4. Discussion of process parameters

To establish an analysis framework of the process, and to describe the influence of its main parameters, numerical models were developed from the FE results of the tube expansion with plate fins (validated by the experimental tests). Among the variables that affect the mechanical expansion process, the following were studied:

- the influence of the friction coefficient f between the ogive and the inner surface of the tube;
- the tube thickness t_0;
- the insertion speed v.

These input factors were changed according to the multilevel factorial design reported in Table 2, and all the 24 possible combinations were simulated. The internal diameter of the tube was set to D_i = 13.85 mm, in order to retain the same geometry and dimensions of the ogive (D_o = 14.5 mm). The external diameter D_e was changed to obtain the imposed wall thickness.

Factor	**Levels**
Friction coefficient, f	0.15; 0.30; 0.45; 0.60
Insertion speed, v (mm/s)	50; 100; 150
Tube thickness, t_0 (mm)	1.0; 1.5

Table 2. Levels of variation of factors.

Moreover, since the expansion ratio is expected to be one of the most important factors influencing the driving force and the tube-fin contact status, for the case of friction coefficient f = 0.15 and speed v = 100 mm/s, and for both the tube thicknesses (t_0 = 1 and 1.5 mm), ogives with four different diameters (D_o = 14.5, 15, 15.5 and 16 mm) were hypothetically considered in the numerical models. It is worth pointing out that, for the maximum ogive diameter D_o = 16 mm, the effective plastic strain in the expanded tube was below the limit of the material.

For each case, the axial and radial components of the driving force were acquired as a function of the ogive stroke l (Fig. 6 *a*). It comes out that the radial driving force is always greater than the axial driving force. The average force values, reported in Fig. 6 *b-c*, were calculated by considering the steady-state region (conventionally, for $l \geq 20$ mm). Fluctuations due to numerical inaccuracies led to standard deviations at most of 1.8 % of the average forces. The combined effect of the axial and radial driving forces influences the value of the resultant force R exchanged between ogive and tube. The modulus of the resultant force and the angle α (measured clockwise from the radial axis) were calculated, and the results are reported in Fig. 7.

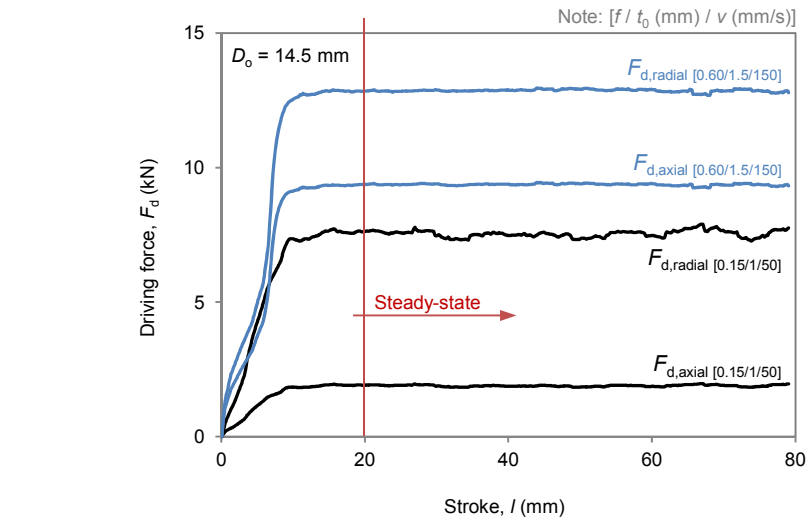

(*a*)

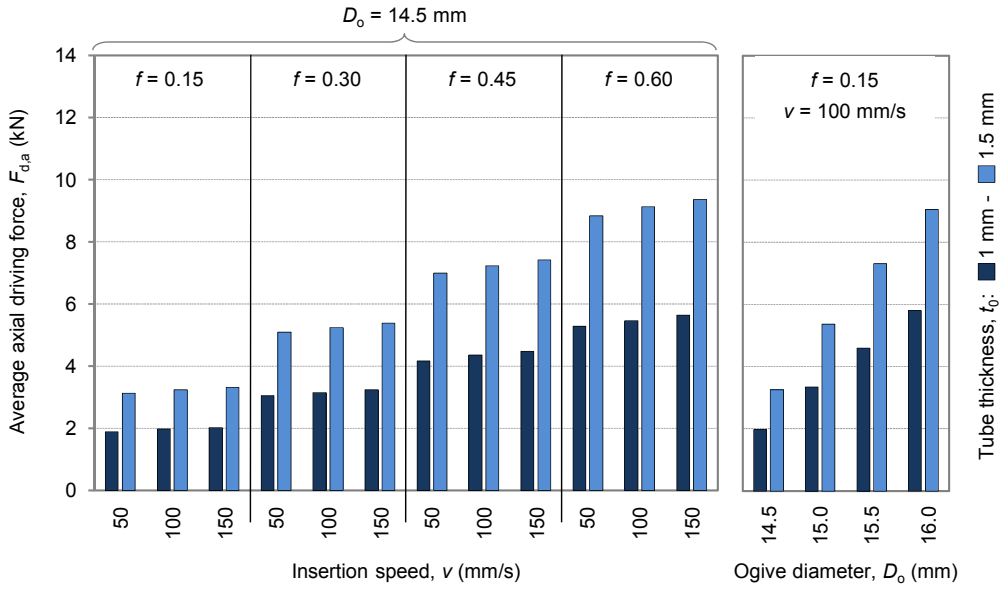

(*b*)

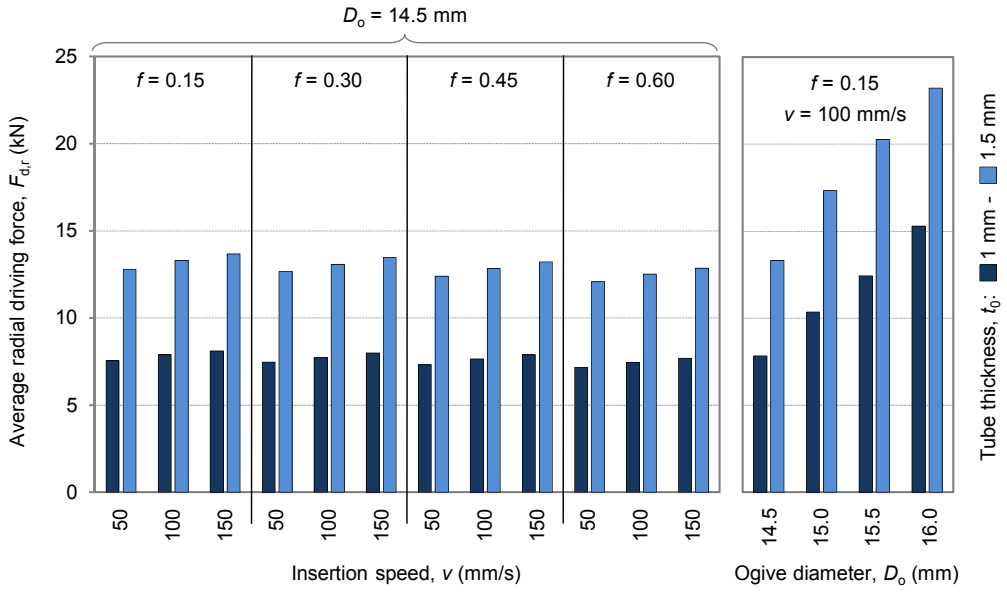

(*c*)

Fig. 6. Driving force results (*a*): average axial (*b*) and radial (*c*) force components as a function of process parameters.

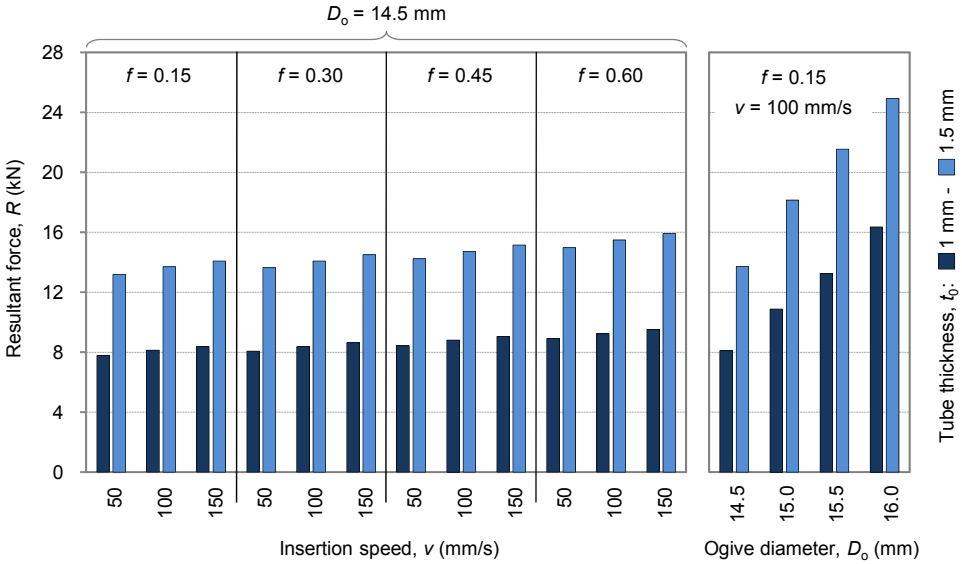

(*a*)

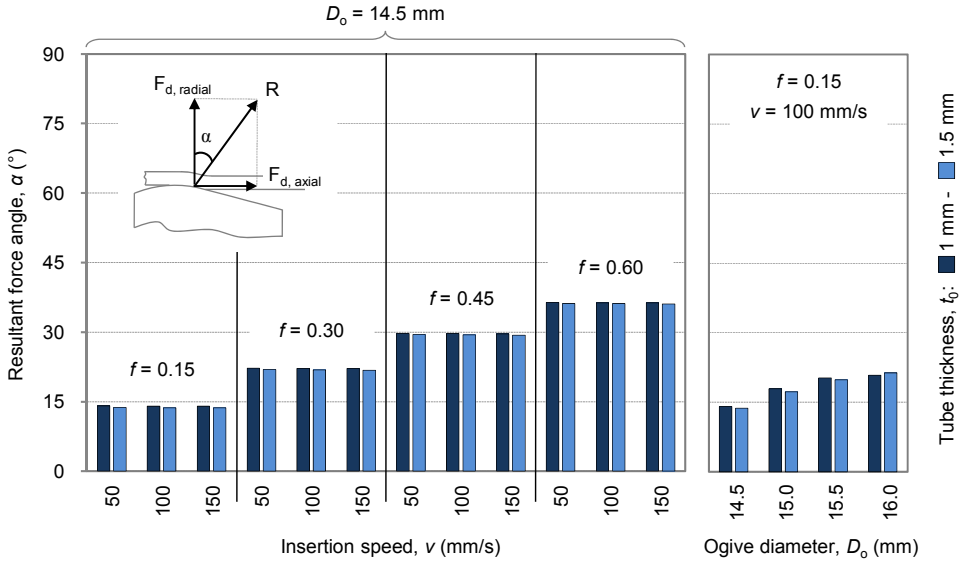

(*b*)

Fig. 7. Influence of process parameters on resultant driving force modulus (*a*) and angle (*b*).

The inner diameter D_i and the final thickness t of the deformed tube were evaluated in 10 sections equally-spaced in the axial direction, from the beginning to the end of the tube. The average values of the measurements were calculated, and the standard deviation was around 2.9% for the thickness t, and 1.1% for the inner diameter D_i. The results are plotted in Fig. 8: all the values are presented as percentage deviations from the nominal values, assumed as reference.

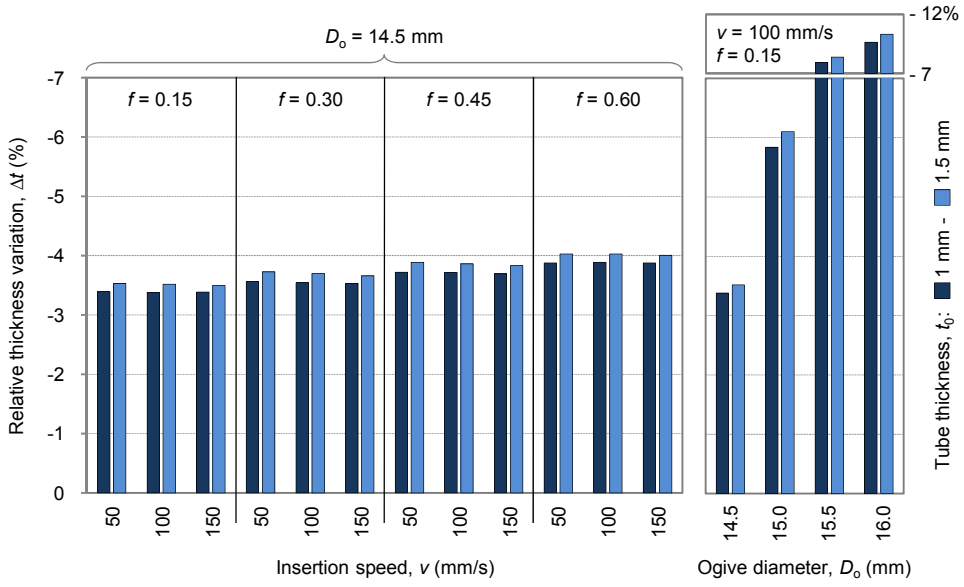

(*a*)

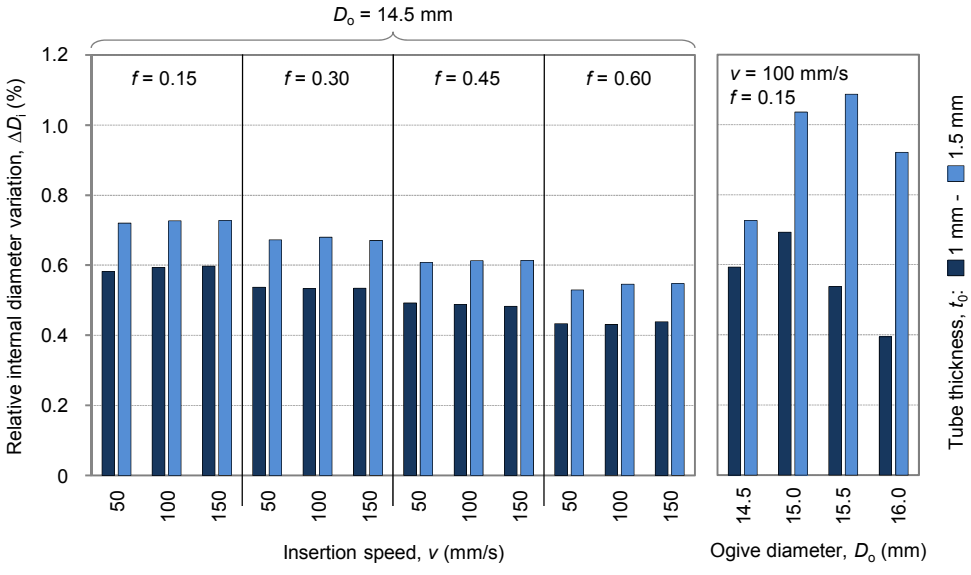

(*b*)

Fig. 8. Influence of process parameters on thickness (*a*) and tube inner diameter (*b*) variations.

For the case of friction coefficient $f = 0.15$, speed $v = 50$ mm/s, ogive diameter $D_o = 14.5$ mm and tube thickness $t_0 = 1$ mm, Fig. 9 *a* shows the radial contact force as a function of the stroke, for 5 different tube/fin contact areas equally spaced. In all curves there is a peak at the beginning that corresponds to the transit of the ogive in close proximity of the fin; afterwards a minimum phase follows, due to the springback phenomenon, and then the contact force settles around an almost constant value. The average values of the steady-state radial contact forces were calculated, and Fig. 9 *b* summarizes the results for all the considered conditions. The standard deviation of the 5 measurements was generally less than 10% of the average value.

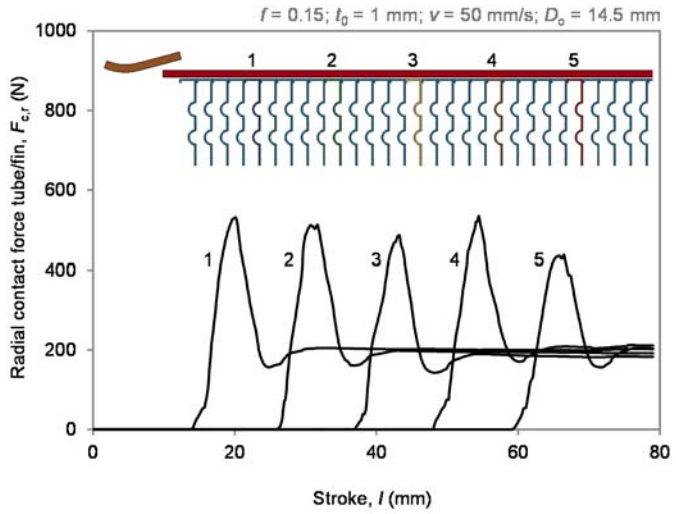

(*a*)

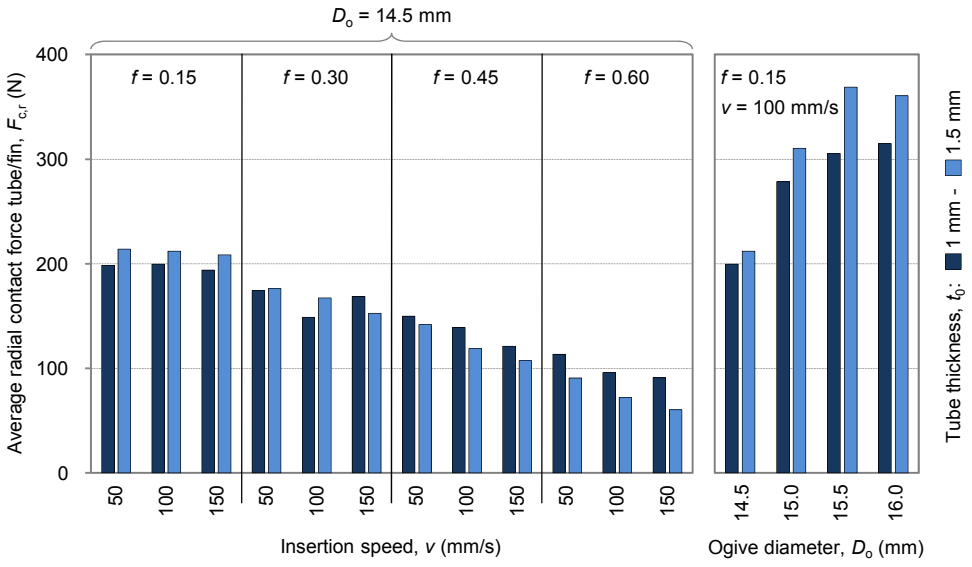

(*b*)

Fig. 9. Radial contact forces exchanged between tube and fins for five different axial positions (*a*), and as a function of process parameters (*b*).

Finally, for the same contact areas defined in Fig. 9 *a*, the maximum gap g_{max} between the inner face of the fin and the external tube wall was evaluated. The obtained average values are presented in Fig. 10. The standard deviation of the 5 measures was around 20% for all the cases. This relatively great scatter can be attributed to the different deformed shapes that the fins (which are in contact one another) assume during the progressive expansion of the tube. In the following, the effect of each factor is discussed.

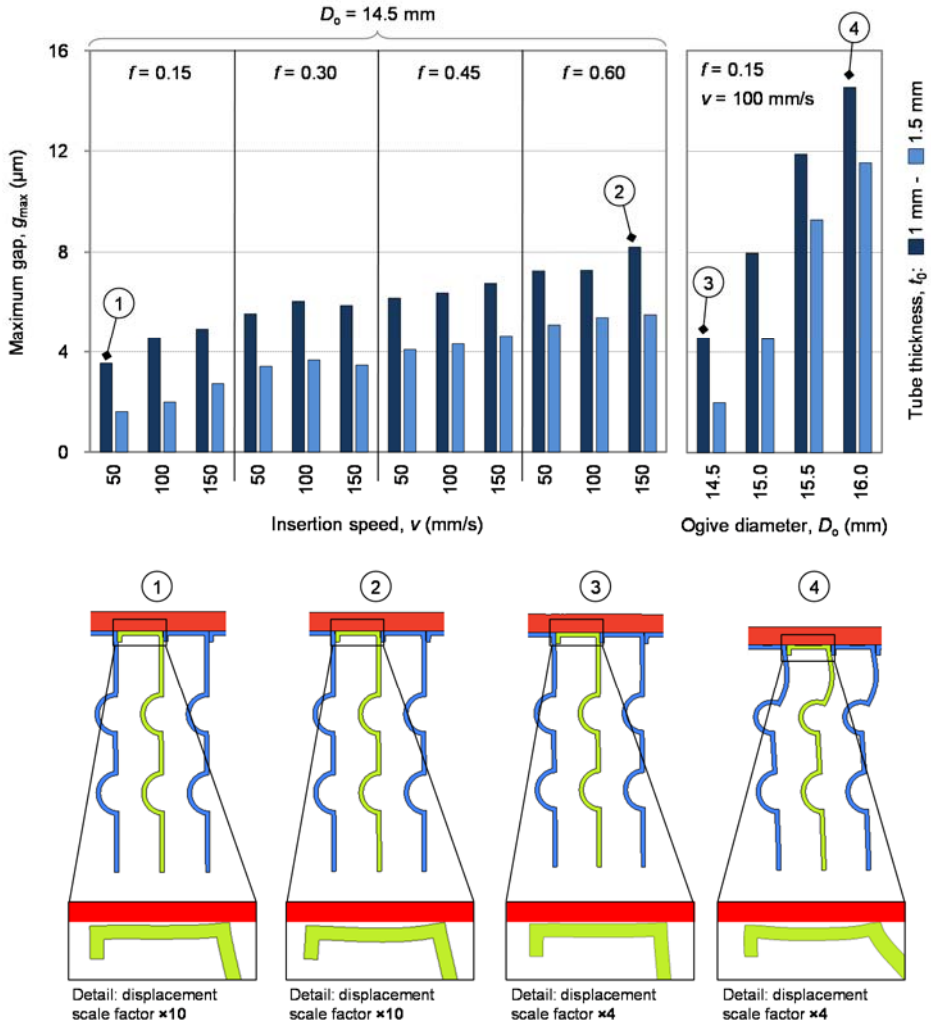

Fig. 10. Analysis of the maximum tube-fin gap.

4.1. Friction coefficient

The numerical analyses reveal that, when the friction coefficient *f* increases, the axial driving force $F_{d,a}$ considerably increases, whilst the radial component $F_{d,a}$ remains almost unchanged (Fig. 6). As a result, being $F_{d,a}$ the principal component of the resultant force (Fig. 7), the modulus of *R* slightly increases with the increase of the friction coefficient *f*. Conversely, the friction is the only factor affecting the inclination of the vector *R*. The angle α increases with the increase of the friction coefficient *f*, and this is due to the expected increase of the frictional force, axially directed,

which opposes the motion of the ogive. As it can be inferred from Fig. 8, thickness and internal diameter variations decrease, in the order of magnitude of tens of microns, when the friction coefficient f is increased. The tube undergoes a minor expansion at higher friction values, due to the increase of the energy dissipated by friction. The smaller expansion of the outer diameter of the tube D_e ($D_i + 2 \cdot t$) influences the contact pressure between tube and fins (Fig. 9). The contact force decreases with the increase of the friction coefficient f, and this should be due to the reduced expansion of the tube. As a consequence, the maximum gap g_{max} increases (Fig. 10, on the left hand side).

4.2. Insertion speed

The insertion speed v, at least within the selected range, induces less significant variations on the expansion process. As far as the driving force is concerned, the components $F_{d,a}$, $F_{d,r}$ (Fig. 6) and the resultant R (Fig. 7) slightly raise with the increase of v, whilst the effect of the insertion speed on the angle α appears to be negligible. With respect to the influence on the tube expansion, relative thickness and diameter variations were not detected (Fig. 8). A limited reduction of the contact force due to the increase of the insertion speed v is appreciated for higher values of the friction coefficient: the conclusions are the same for both the considered thicknesses (Fig. 9). Moreover, a moderate gap increase is also due to the insertion speed v increase (Fig 10).

4.3. Ogive diameter (expansion ratio)

The increase of the expansion ratio have been studied by increasing the ogive diameter up to D_o = 16 mm. These variations give the most significant changes in the results. As expected, the increase of the diameter D_o leads to a considerable increase of the axial and radial driving forces (Fig. 6), as well as of the resultant force R (Fig. 7). The subsequent increase of the angle α reveals that the raise of the axial force is greater than the raise of the radial component. The deformations of the tube and of the fins are also heavily affected by the expansion ratio. The increase of the ogive diameter leads to the increase of the relative thickness variation, which is the ratio of the thickness variation (t-t_0) and of the undeformed tube thickness t_0. In other words, the increase of the ogive diameter leads to the reduction of the tube thickness, as the internal diameter of the tube becomes larger (Fig. 8). The radial contact force exchanged between tube and fin increases with the increase of the ogive diameter (Fig. 9), and the maximum gap g_{max} also increases (Fig. 10). This latter evidence can be explained by observing the deformed shape of the fins, as reported in Fig. 10: with D_o = 16 mm it is evident that the fins are markedly deformed even outside the contact area with the tube, and this modifies significantly the tube-fin packing. This phenomenon was not detected while varying the other process parameters (f, v, and t_0) for the lower ogive diameter D_o = 14.5 mm. According to these results, the choice of the ogive diameter D_o = 14.5 mm leads to better performance in terms of process forces reduction, and the power consumption is

consequently reduced. This effect could drive to the use of smaller machines for the production process. Moreover, being the tube-fin gap reduced for D_o = 14.5 mm, a better heat exchange is expected.

4.4. Tube thickness

The conclusions given in the previous paragraphs can be applied to both the tube thicknesses considered in this study. The FE analyses also demonstrate that an increase in the force magnitude can be related directly to the change of the tube thickness t_0 from 1 mm to 1.5 mm (Figs. 6 and 7 *a*), whilst the results in terms of angle α are comparable (Fig. 7 *b*). The relative tube thickness variations are generally higher for t_0 = 1.5 mm, and in Fig. 8 *b* these differences are exacerbated when increasing the ogive diameter. At lowest friction (f = 0.15), the average radial contact force between tube and fins is slightly higher for t_0 = 1.5 mm, and this trend is reversed at higher friction (Fig. 9). The reasons for this result are not clear, but the small amount of variation does not seem to be worth of further investigations. Finally, for the increased thickness, the maximum tube/fin gap is reduced (Fig. 10).

5. Conclusions

An analysis of the mechanical tubes expansion process for the production of heat exchangers was carried out. The activity needed an experimental characterization of both the materials and the process. The development of 2D axisymmetric FE models allowed a significant reduction in the calculation time compared to a full FE solid model. The numerical model satisfactorily predicts the examined process. There was good agreement between numerical and experimental results of the driving force. This parameter is particularly important in terms of energy consumption, and therefore of manufacturing costs. The mechanical expansion process was also examined and described with the proposed model, and thus the technological parameters allowed the control and optimization of the production process of the heat exchangers. The influence of several parameters (the friction coefficient between the ogive and tube, the wall thickness, the ogive insertion speed, the expansion ratio) on the process (the driving force, the tube thickness, the tube-fin gap) was evaluated. The results confirm that the expansion ratio has the highest impact on the driving force and on the tube-fin contact status. Moreover, the production process performances could be improved through friction reduction between the tube and ogive. A study of the lubrication conditions is therefore needed in order to retain limited driving forces, which could results in lower process energy consumption, and a reduction of the gap between the fin and the expanded tube. This should also improve the heat exchange efficiency, as shown by Madhusudana and Cheng (2007).

Acknowledgments

The research activities were performed with the co-operation of Astra Refrigeranti SpA (Alessandria, Italy). This work was funded by “Regione Piemonte” in the program: “Innovation Voucher 2010 (I0024) -Asse II del Piano Straordinario per l’Occupazione, Misura II.1”.The authors kindly acknowledge for the technical and economical contributions. The authors wish to thank also Angioletta Rita Catalano for the contribution to this work during the development of her B.Sc. thesis.

References

Almeida B.P.P., Alves M.L., Rosa P.A.R., Brito A.G., Martins P.A.F., 2006. Expansion and reduction of thin-walled tubes using a die: experimental and theoretical investigation. International Journal of Machine Tools & Manufacture 46, 1643–1652.

Alves M.L., Almeida B.P.P., Rosa P.A.R., Martins P.A.F., 2006. End forming of thin-walled tubes. Journal of Materials Processing Technology 177, 183–187.

ASTM E8M, 1998. Standard test methods for tension testing of metallic materials.

Cowper G.R., Symonds P.S., 1957. Strain hardening and strain rate effect in the impact loading of cantilever beams. Brown University, Division of Applied Mathematics report 28.

Karrech A., Seibi A., 2010. Analytical model for the expansion of tubes under tension. Journal of Materials Processing Technology 210, 356–362.

Li H.F., Qian C.F., Yuan Q.B., 2010. Cracking simulation of a tubesheet under different loadings. Theoretical and Applied Fracture Mechanics 54, 27–36.

LS-DYNA Keyword User's Manual, version 971. Livermore Software Technology Corporation (LSTC), Livermore, California 94551.

Madhusudana C., Cheng W.-W., 2007. Decrease in thermal contact conductance and the contact pressure of finned-tube heat exchangers assembled with different size bullets. Journal of Heat Transfer 129, 907-911.

Nadai A., 1950. Theory of flow and fracture of solids, 2nd edition. McGraw-Hill Book Company Inc., New York.

Seibi A.C., Barsoum I., Molki A., 2011. Experimental and numerical study of expanded aluminum and steel tubes. Procedia Engineering 10, 3049–3055.

Tang D., Li D., Peng Y., 2011. Optimization to the tube–fin contact status of the tube expansion process. Journal of Materials Processing Technology 211, 573–577.

Tang D., Peng Y., Li D., 2008. An experimental and numerical study of the expansion forming of a thick-walled microgroove tube. Proc. of the Institution of Mechanical Engineers, Part C: Journal of Mechanical Engineering Science 223, 689.

Tang D., Peng Y., Li D., 2009. Numerical and experimental study on expansion forming of inner grooved tube. Journal of Materials Processing Technology 209, 4668–4674.